Q. J. R. Meteorol. Soc. (2000), **126**, pp. 3013–3040

Use of GPS/MET refraction angles in three-dimensional variational analysis

By X. ZOU[1]*, B. WANG[1,2], H. LIU[1,2], R. A. ANTHES[3], T. MATSUMURA[4,5] and Y.-J. ZHU[4]

[1]*Florida State University, USA*
[2]*Institute of Atmospheric physics, China*
[3]*University Corporation for Atmospheric Research, USA*
[4]*National Centers for Environmental Prediction, USA*
[5]*Japan Meteorological Agency, Japan*

(Received 8 April 1999; revised 8 March 2000)

SUMMARY

The Spectral Statistical Interpolation (SSI) analysis system of the National Centers for Environmental Prediction (NCEP) is modified to include GPS/MET data (meteorological data from the Global Positioning Satellite system) using a GPS ray-tracing operator. The new system is tested by incorporating 30 actual GPS/MET observations of refraction angles obtained during the GPS/MET experiment. This is the first time that real radio occultation refraction angles and refractivities have been incorporated into a three-dimensional variational analysis system. We examine the magnitude and the vertical distribution of the analysis adjustments that result from using refraction-angle observations in the NCEP SSI analysis system. The average magnitudes of the adjustments in the temperature and specific-humidity fields are approximately 0.4 degC and 0.6 g kg^{-1}, respectively. Individual changes can be as large as 4 degC and 4 g kg^{-1}, respectively. The greatest adjustments to the temperature occur in the middle and upper troposphere and stratosphere, while the major changes in specific humidity occur in the lower troposphere.

An assessment of the impact of the GPS/MET observations on the analysis, verified by conventional (mostly radiosonde) data, is difficult because of the small number of GPS/MET data used. Nevertheless, it is found that, even over data-rich regions (regions containing many radiosonde observations), and even when the verification data were the radiosonde data themselves, the use of GPS/MET refraction angles makes a slight improvement, overall, to the analysed temperatures and winds. The impact on the water-vapour analyses, again as measured against radiosonde data, is mixed, with improvements shown in some layers and degradation in others. Compared with the background field, the use of refraction angles from one occultation results in an analysis whose simulated refraction angles are much closer to the withheld GPS/MET refraction angles at the two nearby occultation locations, and whose temperature and moisture profiles are also closer to those resulting from the direct assimilation of the two withheld occultations.

Although the forward model used in this study, with the ray tracing being carried out in a two-dimensional plane, is much cheaper than a more accurate three-dimensional forward model, it is still quite expensive. In order to further reduce the computational requirement for the assimilation of GPS/MET data, we test a scheme in which the GPS/MET-retrieved refractivities (instead of refraction angles) are used above a selected height for each occultation. These heights are determined objectively based on the departures from spherical symmetry of the model field. It is shown that the mixed use of GPS/MET refraction angles and refractivities produces an analysis result similar to the one using refraction angles alone, while the computational cost is reduced by more than 30%.

KEYWORDS: GPS/MET refraction angles Ray tracing Variational analysis

1. INTRODUCTION

Since the first launch of a GPS/MET (meteorological data from the Global Positioning Satellite system) instrument package (receiver) carried on a small Low Earth Orbit (LEO) satellite named MicroLab-1, a major goal has been to demonstrate the potential value of these (and future) GPS occultation measurements to numerical weather analysis and prediction. A number of studies have compared the GPS/MET-retrieved temperature profiles with other types of data, such as operational global analysis, radiosondes and other satellite data (Ware *et al.* 1996; Kursinski *et al.* 1996, 1997; Rocken *et al.* 1997). These studies suggest that GPS/MET occultation measurements are accurate and have the potential to be useful in numerical weather prediction (NWP) and climate studies. While a single satellite (MicroLab-1) could not produce enough data globally to improve NWP forecasts substantially, these preliminary GPS analyses have encouraged future efforts to launch many LEO satellites that will provide much more GPS data

* Corresponding author: Florida State University, Tallahassee, Florida, USA.

globally. An immediate question is how these new data will affect global analyses and possibly change the need for other types of observational data. Before one can answer this question, a method that can extract useful information from these measurements needs to be developed and tested using an operational analysis system. Following work by Zou *et al.* (1999), the work presented in this paper summarizes our second step toward incorporating these new GPS occultation data into a global analysis system.

While the results of GPS temperature retrievals cited above demonstrate the potentially useful temperature and geopotential-height information contained in the GPS occultation measurements, the manner in which the moisture information is extracted and how to best use GPS occultation measurements in the global analysis for NWP remains to be seen. The GPS/MET data retrieval method described by Ware *et al.* (1996) and Rocken *et al.* (1997) transforms the observations into analysis (model) variables of temperature and water-vapour pressure. Such a procedure is under-determined. For example, the refraction angle is used to derive information about temperature, specific humidity and pressure. Approximations and some ad hoc assumptions are usually introduced into the retrieval procedure. These include the assumption of spherical symmetry in the Abel inversion, the dry-atmosphere assumption (omission of water vapour) or the use of independently obtained water vapour for the temperature retrieval, and assumptions on the (upper) boundary conditions. The observational information may thus be contaminated by errors inherent in the retrieval procedure due to the use of those assumptions. Since the characteristics of these errors are difficult to calculate and usually not available, the use of these GPS retrieval products (temperature and/or moisture) in an operational analysis system may not allow as much useful information to be extracted as does the direct use of refraction angles in the analysis (Eyre 1994).

Fortunately, many major operational NWP centres incorporate a variety of observations into an analysis system using some form of variational approach (Parrish and Derber 1992; Courtier *et al.* 1994; Zupanski and Zupanski 1995; Rabier *et al.* 1998b). The variational approach allows the direct inclusion of observational information if one can transform the analysis (model) variables into the same form as the observational quantities (Le Dimet and Talagrand 1986; Navon *et al.* 1992). The GPS observations are blended with the background information and other available observations (surface data, radiosonde data, etc.) in a consistent manner, and their influence can be extended in both the horizontal and vertical, as well as to other analysis variables not directly associated with GPS/MET measurements (such as wind) through the multivariate nature of the data analysis system. One such system is the Spectral Statistical Interpolation (SSI) analysis scheme implemented in June 1991 at the National Centers for Environmental Prediction (NCEP) (Parrish and Derber 1992). The NCEP's SSI analysis system is very similar to the three-dimensional variational (3D-Var)/four-dimensional variational scheme used at the European Centre for Medium-Range Weather Forecasts (ECMWF) (Andersson *et al.* 1998; Courtier *et al.* 1998; Rabier *et al.* 1998a,b).

Over the past few years, several efforts have been made to assess the potential impact of GPS data on NWP. Initially, the impact of atmospheric refractivity on temperature and moisture retrieval, and the subsequent model predictions, was assessed (Zou *et al.* 1995; Kuo *et al.* 1997). The atmospheric refractivity can be retrieved from the refraction-angle measurements of GPS occultations under several assumptions (for instance, the assumption of spherical symmetry). The departures from spherical symmetry of the atmosphere cause the GPS-retrieved refractivity to be different from the (local) atmospheric refractivity. Data-analysis experiments which directly incorporate the GPS-retrieved refractivity, although better than the use of the GPS dry-temperature retrieval products (see Ware *et al.* 1996), may still not fully exploit the observational information

of the direct use of GPS refraction angles (Eyre 1994). It has thus become necessary to consider assimilating observations of the refraction angles. As a result, a forward observation operator, that transforms the analysis variables into refraction angles and other related components (such as the adjoint of the ray tracing) needed for the direct use of the refraction angles in the framework of variational analysis, was developed and tested in Zou *et al.* (1999).

In this work, we incorporate GPS/MET refraction-angle measurements into the NCEP SSI analysis system. The basic theory of the use of GPS data within the NCEP SSI system is briefly discussed in section 2. Analysis results, with and without GPS refraction angles, are presented in section 3. Section 4 discusses a proposed mixed use of GPS/MET refractivity and refraction angles aimed at reducing the computational cost while retaining a reasonable accuracy in the final analysed fields. The paper concludes in section 5.

2. Description of the three-dimensional variational data-assimilation experiments

(*a*) *Mathematical formulation of the three-dimensional variational problem*

NCEP's SSI analysis system minimizes an objective function (Parrish and Derber 1992)

$$J(\mathbf{w}) = \underbrace{\tfrac{1}{2}\mathbf{w}^{\mathrm{T}}\mathbf{w}}_{J_b} + \underbrace{\tfrac{1}{2}\{\mathbf{y}_{\mathrm{obs}} - \mathrm{R}(\mathbf{x}_b + \mathbf{C}\mathbf{w})\}^{\mathrm{T}}\mathbf{O}^{-1}\{\mathbf{y}_{\mathrm{obs}} - \mathrm{R}(\mathbf{x}_b + \mathbf{C}\mathbf{w})\}}_{J_o} \tag{1}$$

where $\mathbf{x}_b$ is a 6 h forecast of analysis variables (the vorticity, the unbalanced part of the divergence, the unbalanced temperature, the logarithm of the unbalanced surface pressure, and the mixing ratio) from the previous cycle of analysis (also known as the background or first guess), and $\mathbf{y}_{\mathrm{obs}}$ is an M-component vector of observations. $\mathbf{O}$ is an $M \times M$ observational error covariance matrix (including both the instrument and the representative errors), R is an observation operator that converts the analysis variables on model grids into the observation quantities and locations, $\mathbf{w} = \mathbf{C}^{-1}(\mathbf{x} - \mathbf{x}_b)$, $\mathbf{C}$ is related to the forecast error covariance matrix $\mathbf{B}$ by $\mathbf{B} = \mathbf{C}\mathbf{C}^{\mathrm{T}}$, and $\mathbf{x}$ $(= \mathbf{x}_b + \mathbf{C}\mathbf{w})$ is an N-component vector of analysis variables. J_b is the background term and J_o the observation term.

Minimization of J is carried out by the following procedure:

1. Minimization of J(w) using a perturbation method:

The minimum of J(w), $\mathbf{w}^*$, satisfies

$$\frac{\partial J}{\partial \mathbf{w}} = \mathbf{w} - \mathbf{C}^{\mathrm{T}}\mathbf{L}^{\mathrm{T}}\mathbf{O}^{-1}\{\mathbf{y}_{\mathrm{obs}} - \mathrm{R}(\mathbf{x}_b + \mathbf{C}\mathbf{w})\}|_{\mathbf{w}=\mathbf{w}^*} = 0 \tag{2}$$

where $\mathrm{L} = \partial \mathrm{R}/\partial \mathbf{x}$ is the tangent linear of the observation operator R. Equation (2) is solved through an iterative procedure (the outer loop). At the first iteration ($k = 1$), $\mathbf{w} = \mathbf{w}_1 = 0$ and $\mathbf{x} = \mathbf{x}_1 = \mathbf{x}_b$. Assume that at the k-th iteration ($k = 1, 2, \ldots$), $\mathbf{w} = \mathbf{w}_k$, $\mathbf{x} = \mathbf{x}_k$. The value of $\mathbf{w}$ at the $(k + 1)$-th iteration, $\mathbf{w}_{k+1}$, is found by adding a small perturbation, $\boldsymbol{\delta}_k$, (to be determined) to $\mathbf{w}_k$, i.e.

$$\mathbf{w}_{k+1} = \mathbf{w}_k + \boldsymbol{\delta}_k \tag{3}$$

2. Solution of a linear equation for the increment at the k-th iteration, $\boldsymbol{\delta}_k$

Substituting Eq. (3) into Eq. (2) gives (retain only the linear terms):

$$\mathbf{w}_k + \boldsymbol{\delta}_k - \mathbf{C}^{\mathrm{T}}\mathbf{L}_k^{\mathrm{T}}\mathbf{O}^{-1}\{\mathbf{y}_{\mathrm{obs}} - \mathrm{R}(\mathbf{x}_{\mathrm{b}} + \mathbf{C}\mathbf{w}_k) - \mathrm{L}_k\mathbf{C}\boldsymbol{\delta}_k\} = 0 \tag{4}$$

or

$$\underbrace{(\mathbf{I} + \mathbf{C}^{\mathrm{T}}\mathbf{L}_k^{\mathrm{T}}\mathbf{O}^{-1}\mathrm{L}_k\mathbf{C})}_{\mathbf{A}(\mathbf{x}_k),\ \text{coefficient matrix}}\ \boldsymbol{\delta}_k = \underbrace{\mathbf{C}^{\mathrm{T}}\mathbf{L}_k^{\mathrm{T}}\mathbf{O}^{-1}\{\mathbf{y}_{\mathrm{obs}} - \mathrm{R}(\mathbf{x}_{\mathrm{b}} + \mathbf{C}\mathbf{w}_k)\} - \mathbf{w}_k}_{\mathbf{f}(\mathbf{x}_k),\ \text{forcing vector}}\ . \tag{5}$$

The above linear equation (with respect to $\boldsymbol{\delta}_k$) is solved through an iteration (the inner loop) using a standard linear conjugate-gradient algorithm.

In the experiments using GPS/MET data, $\mathbf{y}_{\mathrm{obs}}$ is extended to include the refraction-angle observations in the analysis. Since refraction angle is not a basic variable defined on the model grid, it is necessary to include in the R operator an integration of ray trajectory (Zou *et al.* 1999). The tangent linear and adjoint of the ray-tracing calculation are included in L and L^{T}, respectively.

Most computational costs of GPS data analysis come from the repeated applications of R, L and L^{T} operators in the iterative procedure of the minimization employed in the variational data analysis. The use of GPS refraction-angle observations in 3D-Var contains the transforms of analysis variables on the model grids to and from the refraction angles at various perigee points. Specifically, the GPS observation operator that maps the model state vector to the refraction angles involves (i) a ray-tracing procedure solving a ray-trajectory equation in a Cartesian coordinate system from assigned initial conditions (initial ray position and tangent direction, deduced from the GPS observational information of the ray perigee point position and the normal direction of the ray at the perigee point); (ii) routines executing coordinate transfers to and from the geodetic coordinates (z, φ, λ) from and to the local Cartesian coordinates (x_1, x_2, x_3), as well as calculation of the geometrical height (the height above the earth's surface) from the geopotential height; and (iii) calculation of the refraction angle as the angle between the initial and the final tangent vectors of the simulated ray (see Zou *et al.* 1999).

(*b*) *Experiment design*

NCEP's SSI system, briefly described above, was used to run several 3D analyses, including some or all of the GPS/MET refraction angles (a total of 30 occultations) available in a 6 h window centred at 12 UTC 11 October 1995. Figure 1 shows the geographical distribution of these occultations by their mean perigee-point positions. They are numbered in the order of their observing times. For example, the occultation number 2 (denoted GPS-2 hereafter) is received right after occultation number 1 (GPS-1). We mention that these data were obtained when the encryption was turned off. Also shown in Fig. 1 are the 28 radiosonde locations that are close to GPS occultations. The distances from these radiosonde stations to at least one of the GPS/MET soundings are all less than 500 km.

The same background field (GUESS, a 6 h forecast from the prior analysis at 06 UTC 11 October 1995) will be used for all three 3D-Var experiments. We note that the GUESS field contains significant conventional (radiosonde) data information from the 12 hours prior to 12 UTC 11 October. The three analyses are produced using both the 30 GPS refraction angles and the conventional data (radiosondes, marine data, aircraft data, land surface station data, profilers, NEXRAD (NEXt generation RADar) wind data, and scatterometer winds), and referred to as 'BOTH'; the GPS refraction angles only

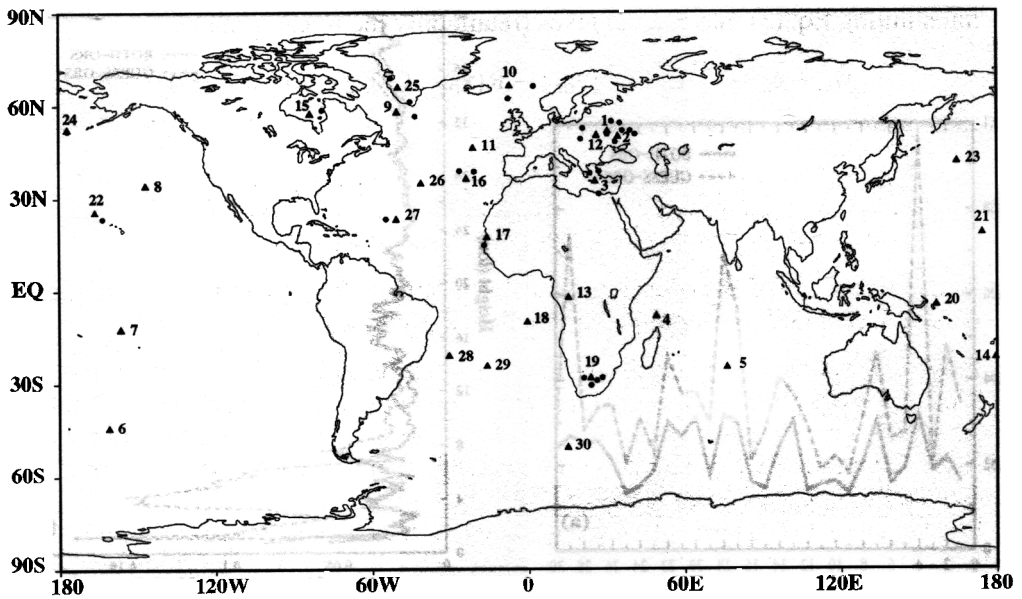

Figure 1. The global distribution of all 30 Global Positioning Satellite (GPS) occultations received from the MicroLab-1 satellite during a 6 h period centred at 1200 UTC 11 October 1995 (triangles). See text for further details.

(ANGLE); and the conventional data only (NOGPS). Three additional experiments, which include only GPS-1, GPS-2 or GPS-12 (ANGLE1, ANGLE2 and ANGLE12), are then conducted to provide additional observational verification of the analysis results from the use of GPS/MET refraction angles. All the data assimilation experiments are carried out at a horizontal resolution of T62L28, which gives approximately 1.9 degrees of resolution.

Note that there are some differences between this experimental version and the current operational version of the SSI system, which is continually changing. In addition, not all of the operational observational data, such as TIROS (Television Infra-Red Observation Satellite) Operational Vertical Sounder (TOVS) radiances, were used in our experiments because they were not readily available.

The refraction angle, α, and its error variance vary exponentially with height. The logarithm of α is, therefore, used as the GPS observational quantity in J. The conversion to $\ln \alpha$ makes the observation errors more homogeneous in the vertical. In contrast, α, and hence its errors, varies by orders of magnitude. The definition of the GPS observational error covariances (in terms of $\ln \alpha$) controls the weighting of various observations. In this research, only the variances are considered. The inclusion of correlated errors, especially in the vertical, will be discussed in future work. The observational error variances are approximated by the mean square differences between the observed and the simulated $\ln \alpha$ based on the background field (see Fig. 2(b), dashed line). Since the observational increments, i.e. observation − guess, contain both the observation errors and the background errors, the observational errors estimated in our study may be higher than the actual ones. The vertical structure of the estimated error variance in the lower troposphere may not represent real fluctuations in observation-error variance and may be caused by the very small sample used here. A vertical sampling (given in Table 1), determined empirically based on the vertical gradient of the atmospheric refractivity profile, is chosen for the forward ray-tracing model.

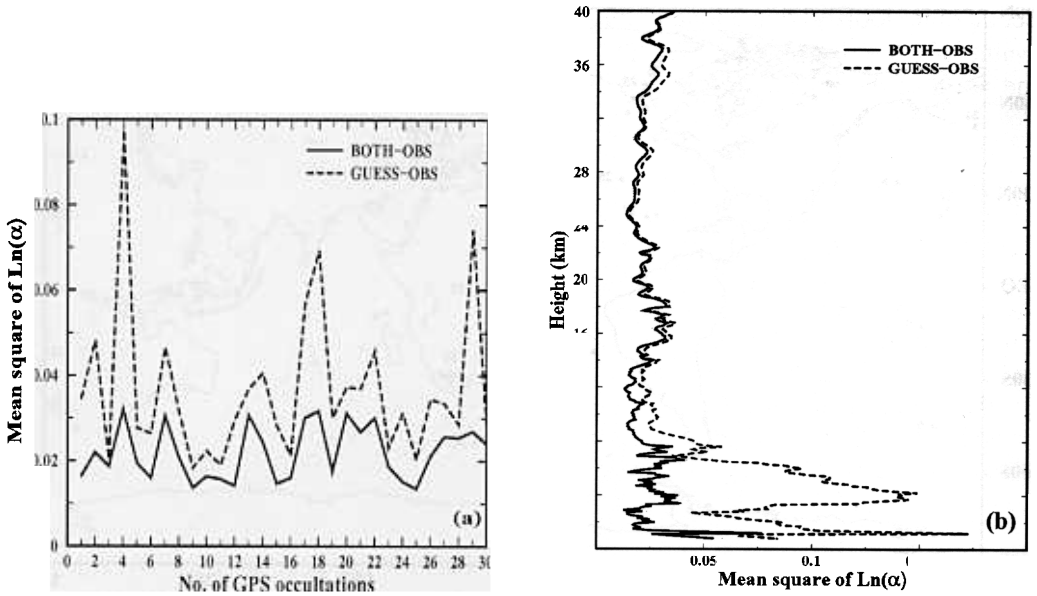

Figure 2. The mean square differences between the simulated and the observed logarithms of refraction angles (ln α) before (GUESS, dashed line) and after (BOTH, solid line) the three-dimensional analysis. (a) Variation with the number of occultations, over all levels. (b) Vertical variation of all soundings.

TABLE I. VERTICAL RESOLUTION OF GLOBAL POSITIONING SATELLITE RAY TRACING

Height (h) (km)	Vertical resolution (km
	2.0
	1.5
	1.0
	0.8
	0.6
	0.4
	0.2

The vertical resolution increases toward the earth's surface; i.e. the closer the ray is to the earth's surface, the higher the vertical resolution. The total number of rays for different occultations varies depending on the height of the model top as well as the lowest perigee height of the ray that does not interact with the Earth's surface before leaving the atmosphere. The average number of rays for each occultation is about 76, of which about 52 rays are calculated below 13.5 km and 15 rays are below 6 km.

3. NUMERICAL RESULTS FROM THE USE OF GPS/MET REFRACTION ANGLES

(*a*) *Convergence*

The objective function Eq. (1) minimized in BOTH includes all 30 GPS/MET occultations and all the conventional data available within ±3 h centred at 12 UTC 11 October 1995. The radiosonde measurements include 682 temperature soundings, 539 specific-humidity soundings, and 1166 wind soundings available in this 6 h time window. Sixty iterations are performed at the first outer loop and 24 iterations at the

second outer loop, giving a total of 84 iterations. The objective function decreased from a value of 2.6×10^4 to 3.8×10^3. The GPS part of the cost function decreased by 79%. The norm of the gradient decreased six orders of magnitude in 84 iterations. Most of the changes resulting from the minimization of the 3D-Var analysis occurred within 21 iterations.

Figure 2 shows the mean square differences of the logarithmic refraction angles between analyses and observations after (solid line) the 3D analysis of the BOTH experiment including all 30 occultations. The mean square difference of $\ln \alpha$ for each occultation (Fig. 2(a)) is calculated for all the rays in the vertical. The values of the mean square differences of $\ln \alpha$ are reduced for all soundings after the 3D analysis, with larger decreases for those soundings where the mean square differences between the background and the observations (dashed line) are larger. If we examine the vertical distribution of the mean square differences of $\ln \alpha$ calculated for all the 30 occultations for both GUESS and BOTH (Fig. 2(b)), we find that the largest reduction in the values of the mean square differences between the simulated and the observed refraction angles occurs at around 5 km.

(*b*) *Analysis increments of ANGLE*

We next examine the vertical profiles of the ANGLE analysis increments interpolated to the GPS/MET occultation locations. Although the average adjustments at the levels where the adjustments are greatest in the refractivity, temperature and specific humidity in ANGLE (also BOTH) are less than 4 N-units, 0.4 degC, and 0.6 g kg^{-1}, respectively, individual changes in the refractivity, temperature and specific humidity after minimization can be as large as 20 N-units, 4 degC, and 4 g kg^{-1}, respectively. Figure 3 shows the 30 vertical profiles of the adjustments of the atmospheric refractivity, temperature and specific humidity produced by the fit to GPS/MET refraction-angle observations. We observe that large adjustments in the refractivity profile (Fig. 3(a)) occur mostly below 6–7 km. Large adjustments in the specific-humidity field are seen in the middle and lower troposphere. The adjustments in the temperature profile appear at all levels. We notice that soundings with large temperature changes (Fig. 3(b)) do not coincide with those having large changes in the specific-humidity profiles. For instance, the adjustment in the temperature profile for GPS-6 is as large as −4 degC near 11 km and 1.8 degC in the entire troposphere below 9 km, while the adjustment in the specific-humidity profile for the same sounding is smaller than 0.2 g kg^{-1} at all levels. In contrast, the adjustment of the specific-humidity profile for GPS-4 is as large as −4 g kg^{-1}, while the largest adjustment in the temperature profile for the same sounding (GPS-4) is smaller than 0.2 degC. We note that GPS-6, which has the greatest adjustments in temperature, is in the southern hemisphere storm tracks where analysis errors are expected to be the greatest.

The distribution of the adjustments in the specific humidity (Fig. 3(c)) below 7 km resembles that of refractivity (Fig. 3(a)). A large adjustment in the refractivity profile (Fig. 3(a)) in the mid and lower troposphere is generally accompanied by a large adjustment in the specific-humidity profile (Fig. 3(c)) at the same level. This is probably a result of the combined effect of a more accurate guess temperature than the guess specific humidity, the similar exponential variation with height of both the atmospheric refractivity and the specific humidity, and a greater sensitivity of refractivity to perturbations in water vapour than to temperature in the lower troposphere (Cacuci 1981; Zou *et al.* 1993).

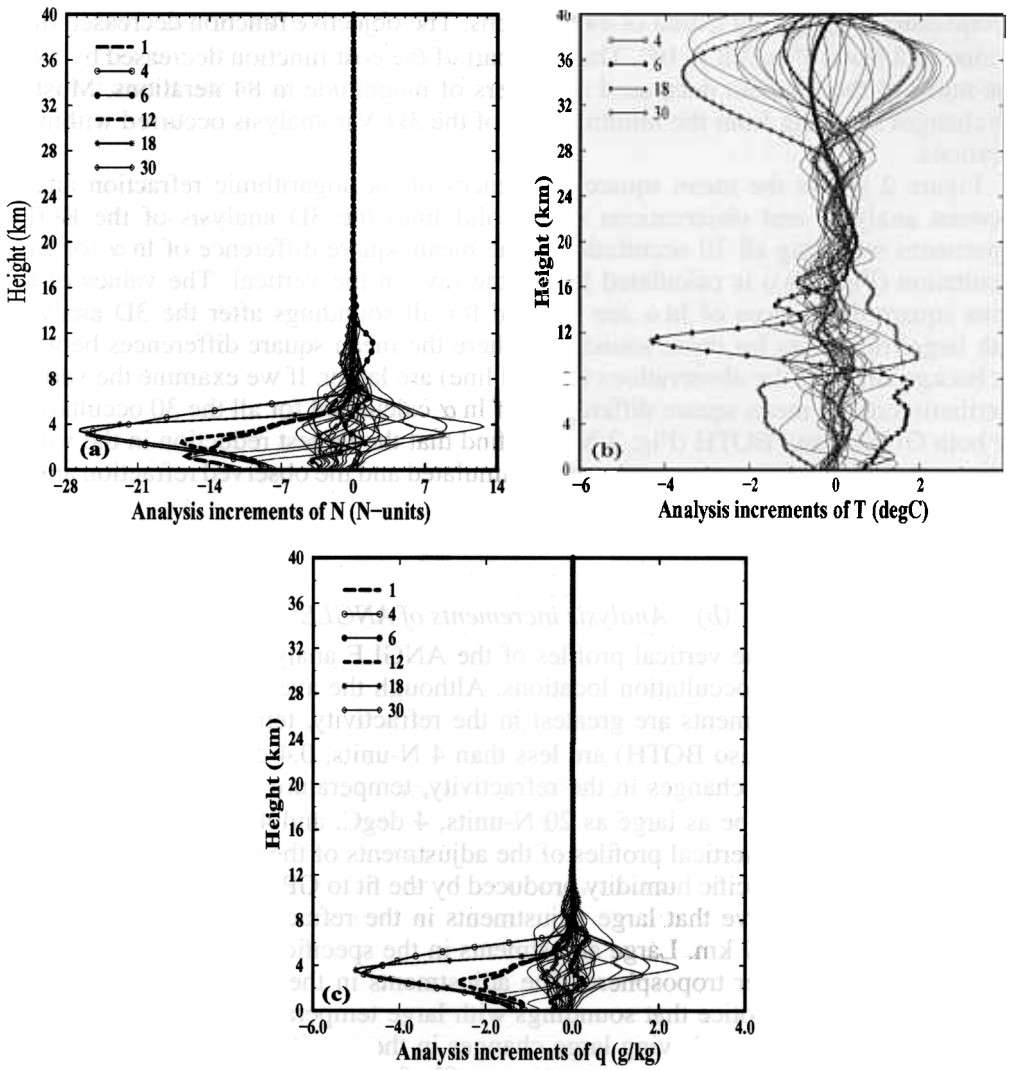

Spaghetti maps showing the 30 vertical profiles of the ANGLE analysis increments of (a) refractivity (N), (b) temperature (T), and (c) specific humidity (q).

We note that large adjustments in the temperature analysis occur above 28 km, a reflection of either a relatively poor large-scale analysis at these heights (possibly due to the lack of TOVS data in our experiments), or the presence of large-amplitude gravity waves in the GPS/MET profiles at these altitudes, as found by Hocke (1997), Kursinski *et al.* (1997) and Tsuda *et al.* (2000). The large magnitude of adjustments of either sign, with little bias, is consistent with temperature perturbations associated with gravity waves. Another factor that may possibly have contributed to the random oscillatory analysis increments at GPS/MET observation locations at high altitudes (>28 km) could be related to GPS/MET observation errors in the upper-boundary conditions and the inadequate removal of ionospheric effects (Hocke 1997). Further study is needed to understand the large temperature adjustments resulting from the GPS/MET data analysis at these high altitudes.

We choose four occultations to illustrate the vertical profiles of the temperature and specific humidity from the ANGLE and GUESS analyses and the GPS 'dry-temperature' retrieval from the University Corporation for Atmospheric Research Payload Operations Control Center (POCC) (Fig. 4). Of the four soundings, two have the largest temperature adjustments (GPS-6 and GPS-30) and the other two have the largest moisture adjustments (GPS-4 and GPS-18). We find a consistent warming of about 1 degC in the troposphere and a strong cooling of about 4 degC near the tropopause for GPS-6 (see also Fig. 3(b)). In addition, we notice a sharp temperature inversion around 12.5 km in both the ANGLE and POCC temperature profiles, which is hardly seen in the GUESS (or NOGPS, not included) profile. A west–east cross-section, cutting through the latitude of GPS-6 (44°S) (Fig. 5), shows a westward dip of the upper-level cold air located to the east of the occultation, causing an additional cooling of about 4 degC near 18 km, compared with the GUESS or the NOGPS analysis. Generally speaking, the ANGLE temperature profiles lie between the GUESS and the POCC profiles (Fig. 4). The temperature difference between POCC dry-temperature retrieval and GUESS is quantitatively larger than the difference between the ANGLE analysis and GUESS. Adjustments in the moisture profiles (right panels) appear mostly in the troposphere below 7–8 km. The large departures of the POCC 'dry-temperature' profiles below 8 km are the result of the omission of water vapour in the computation of temperature from the refractivity (Ware *et al.* 1996). We notice that the use of GPS/MET refraction angles reduced the amount of water vapour in the GUESS field near 3–4 km (about 700 hPa ± 130 hPa) for GPS-4, GPS-18 and GPS-30.

Having examined the vertical distributions of the ANGLE analysis increments, we now examine the horizontal distributions of the increments. The ANGLE analysis data are differenced from the GUESS field and shown in Figs. 6, 7 and 8. Figure 6 shows the temperature differences for σ levels 17, 13 and 8. Large differences occur at several occultation locations. The sign of the temperature differences at the upper level (300 hPa) is opposite to that of the lower (500 hPa and below) troposphere. A negative adjustment at and below 500 hPa is accompanied by a positive adjustment at 300 hPa, and vice versa. Figure 7 shows the specific-humidity differences for σ level 8. Centres of large moisture changes are not generally collocated with those of the temperature differences. Most GPS occultations that cause significant adjustments in the moisture field are located in the tropics between 30°N and 30°S, except for GPS-1 and GPS-12, which are located over Europe. Results from Figs. 3, 4, 6 and 7 suggest that GPS refraction angles often lead to significant changes in the analysis of either temperature or water vapour. It is less often that they contribute significantly to changes in the analysis of both temperature and moisture at a single occultation location. The possible physical and numerical reasons behind this need to be investigated if this still holds true for a larger sample of observations.

The influence of GPS refraction-angle observations extends to wind fields (variables not directly associated with GPS measurements) through the multivariate nature of NCEP's SSI analysis system. Figure 8 shows the wind-analysis increments of ANGLE at σ level 8 centred near the GPS-15 occultation location. Note that the spatial distributions of u and v increments produced by a single GPS occultation should be similar, but not identical, to what would be produced by a single temperature observation. They are the combined effects of the background error structure and the 3D nature of the GPS observation ray-tracing operator, in which the refraction angle depends on the atmospheric refractivity at not only the perigee point, but also along the ray path, causing adjustment in the temperature (and moisture) over a region of several hundred kilometres (~600 km) in radius, centred at the perigee point (see Zou *et al.* 1999).

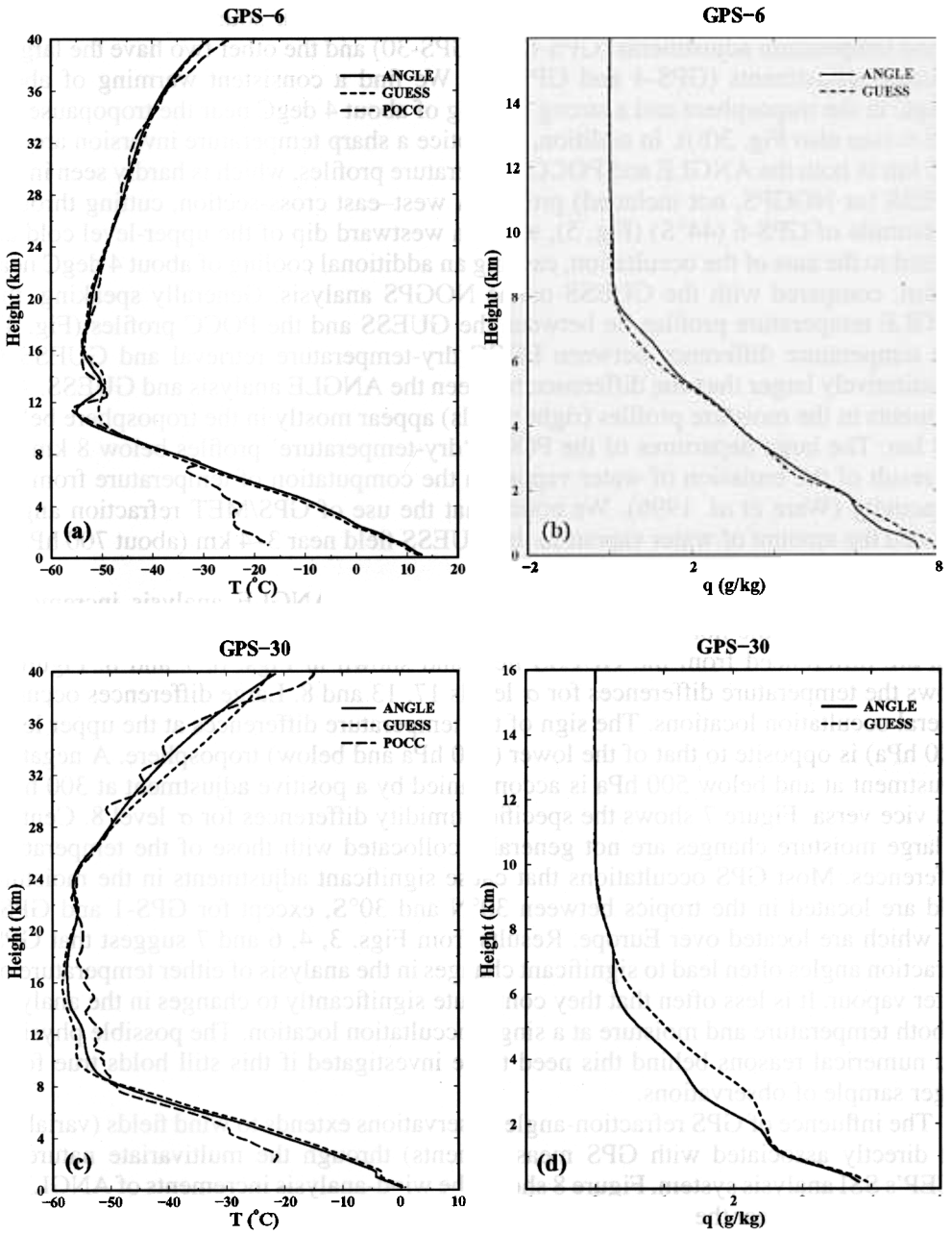

Figure 4. The vertical profiles of the temperature (T) ((a), (c), (e), and (g)) and specific humidity (q) ((b), (d), (f), and (h)) before (GUESS, dashed line) and after (ANGLE, solid line) the three-dimensional analysis and the Global Positioning Satellite (GPS) dry-temperature retrieval (long-dashed line) at four selected GPS occultation locations: GPS-4, GPS-6, GPS-18, and GPS-30.

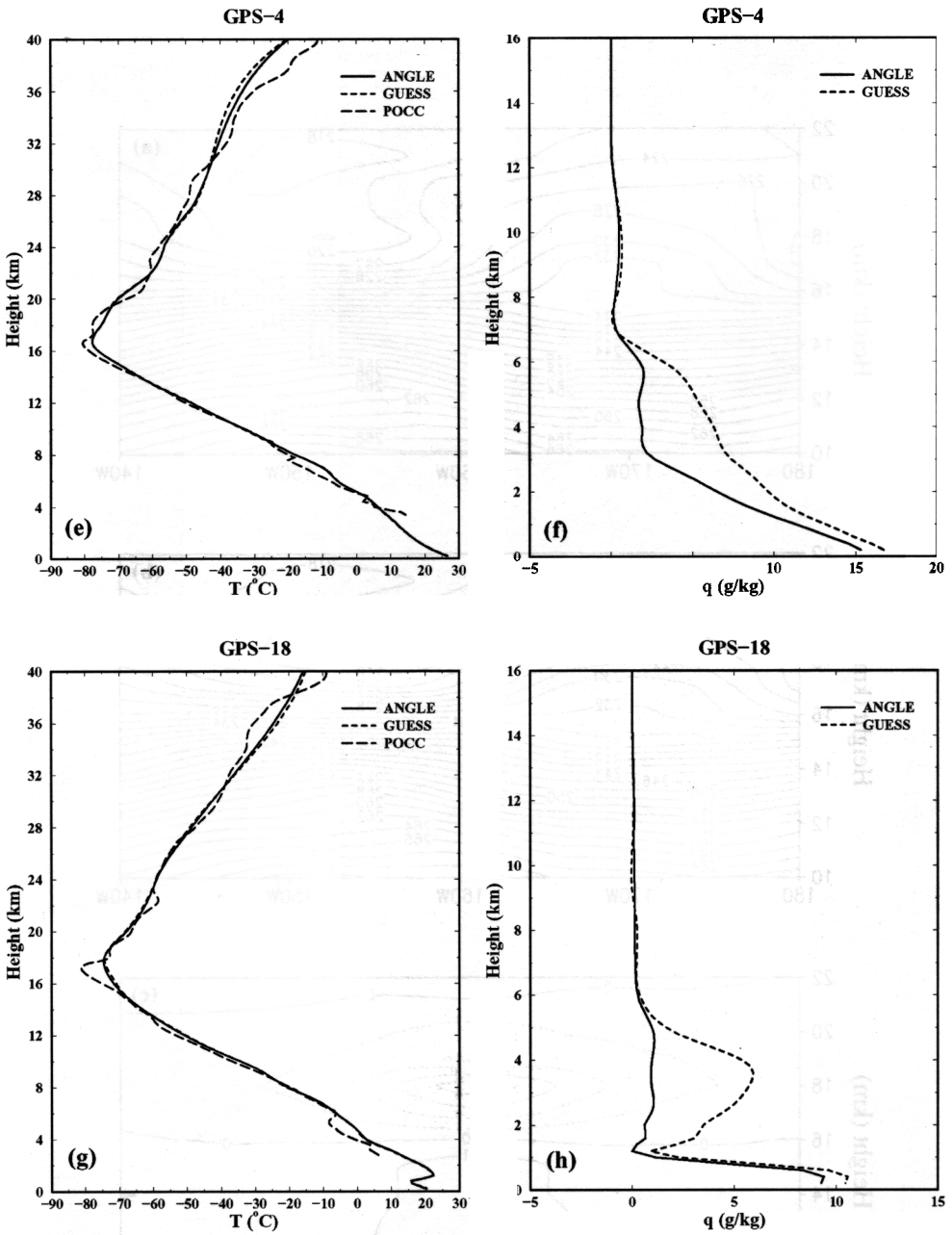

Figure 4 Continued

The forecast error statistics in SSI do not include a correlation between the moisture and the other variables, and the moisture analysis is, therefore, independent of the analysis of the other variables. Analysis differences in the moisture fields over tropical regions, where refraction-angle data had little impact on the temperature field, do not produce any significant changes in the wind fields.

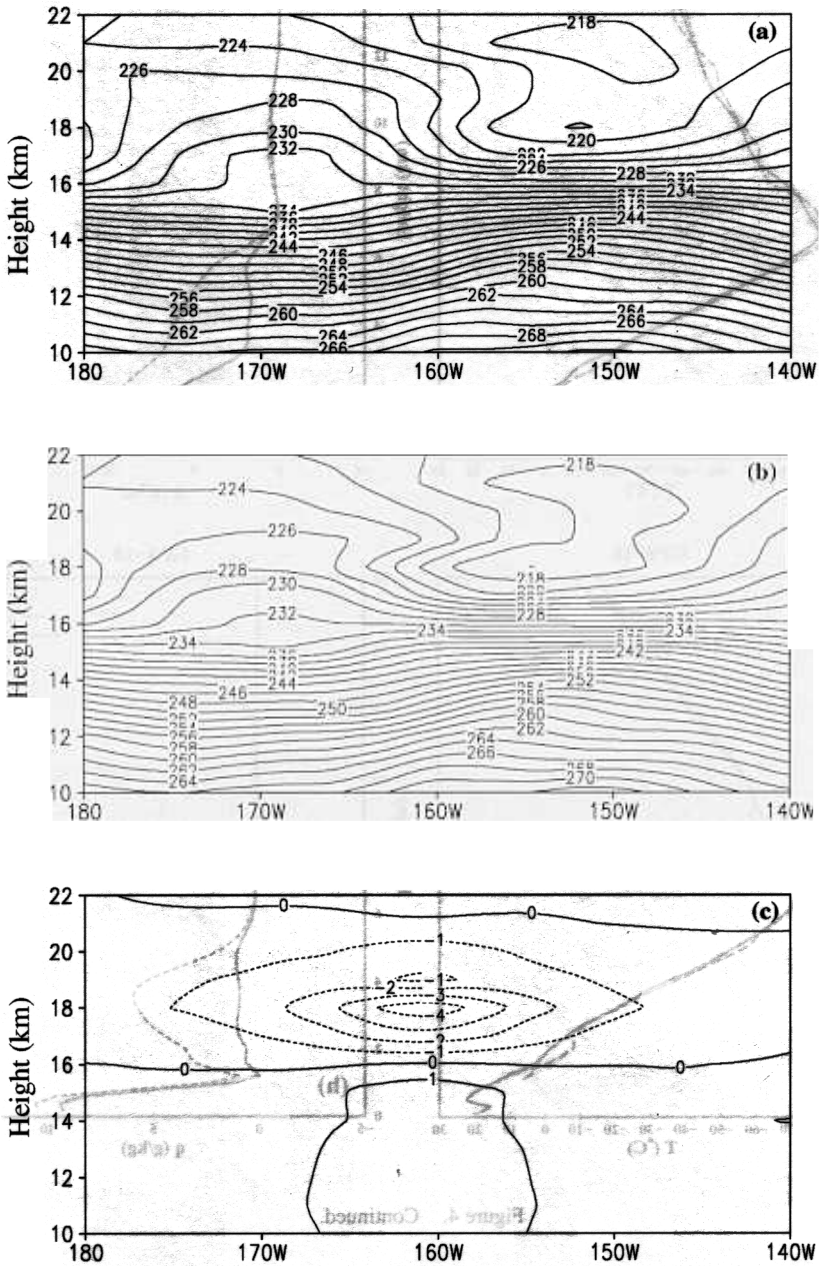

Figure 5. Distribution of the temperature in a west–east cross-section cutting through the latitude of GPS-6 (44°S) for (a) GUESS, (b) ANGLE and (c) ANGLE−GUESS. Contour intervals are 2 degC for (a) and (b) and 1 degC for (c). See text for further details.

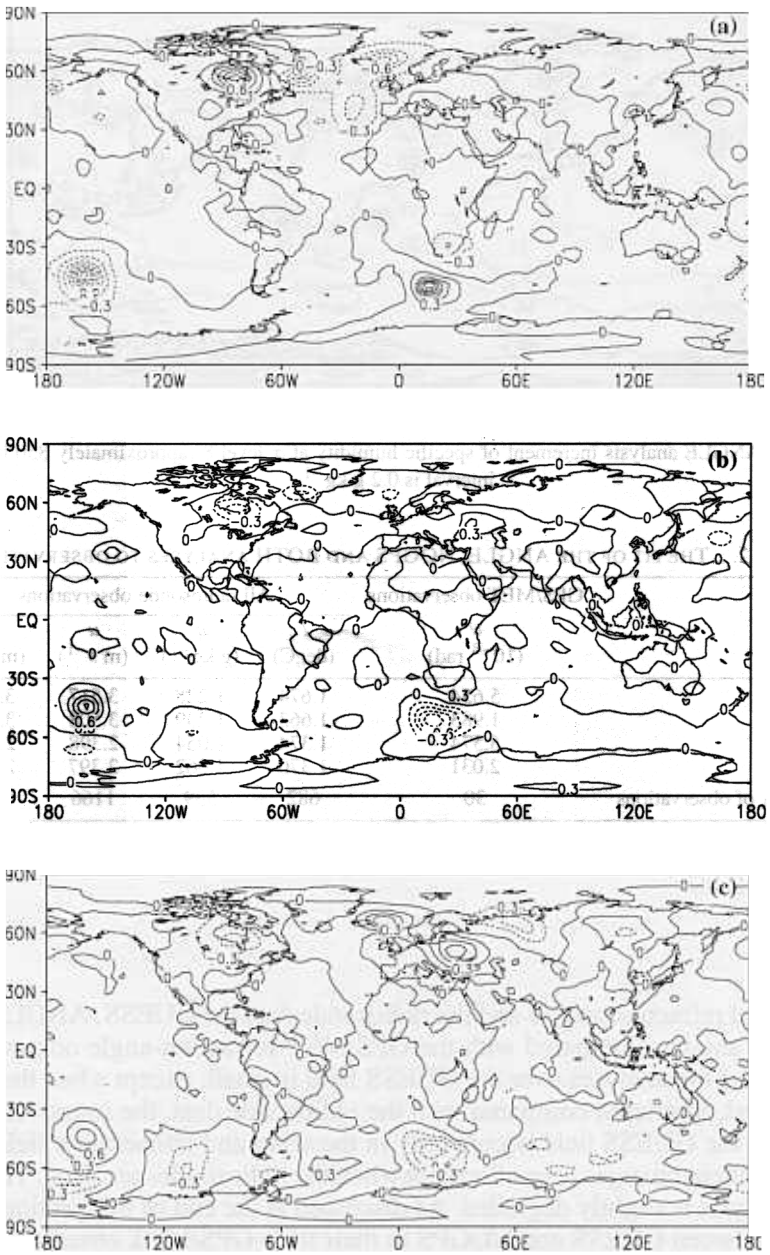

Figure 6. The ANGLE analysis increment of temperature at σ levels (a) 17 (approximately 300 hPa), (b) 13 (approximately 500 hPa), and (c) 8 (approximately 850 hPa). Contour interval is 0.3 degC. See text for further details.

(c) *Comparing ANGLE, NOGPS, and BOTH analyses with radiosondes and refraction-angle data*

Although it is impossible to draw meaningful conclusions about the impact of GPS/MET data on operational analyses and forecasts from one case study using only 30 occultations observed globally, an *indication* of the impact of GPS/MET observations on the analyses can be found from the fit of these analyses to observations. In Table 2, the fit

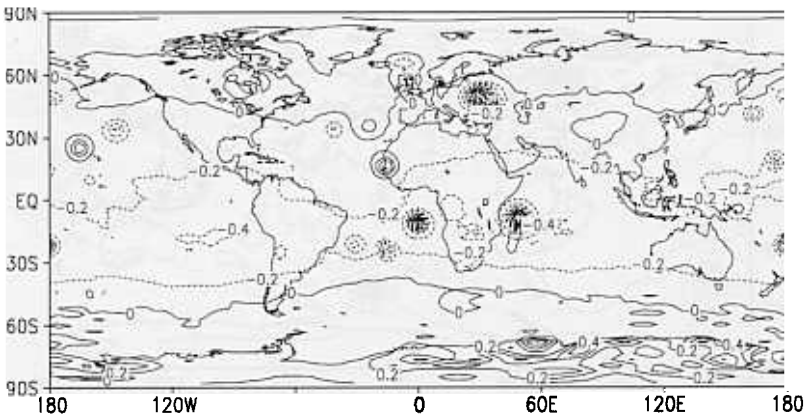

Figure 7 The ANGLE analysis increment of specific humidity at σ level 8 (approximately 850 hPa). Contour interval is 0.2 g kg^{-1}.

TABLE 2. THE FIT OF THE ANGLE, NOGPS AND BOTH ANALYSES TO OBSERVATIONS

Analysis	GPS/MET observations	All radiosonde observations			
	α (10^{-4} rad)	T (degC)	q (g kg^{-1})	u (m s^{-1})	v (m s^{-1})
GUESS	5.654	1.674	1.228	3.517	3.335
ANGLE	1.983	1.663	1.239	3.508	3.323
NOGPS	5.574	1.374	1.054	2.398	2.238
BOTH	2.031	1.370	1.062	2.397	2.238
Number of observations	30	682	539	1166	1166

The numbers are the root-mean-square differences computed over all observed Global Positioning Satellite meteorological (GPS/MET) data or all radiosondes and all levels of each analysis. See text for further details.

to the observed refraction angles and the radiosonde data for GUESS, ANGLE, NOGPS and BOTH is shown. Compared with the GPS/MET refraction-angle observations, the improvement of the analyses over the GUESS field is small, except when the refraction angles are used. Similarly, compared with the radiosonde data, the improvement of the analyses over the GUESS field occurs only in the wind and temperature fields, and the magnitude of these changes is small except when the radiosondes are used. The specific-humidity analysis is slightly degraded. As discussed at the end of this section, the small differences between GUESS and NOGPS in their fit to GPS/MET observations and the small differences between ANGLE and GUESS and between BOTH and NOGPS, when compared with radiosonde data are due to the large differences between the number and location of the radiosonde and the GPS/MET observations.

Because there are many more radiosondes than GPS/MET observations, the adjustments to the analyses, when compared with radiosondes, is very small. Another way to examine how effective the use of refraction angles is in the analysis is to compare the ANGLE and BOTH analyses with only *nearby* radiosonde profiles, instead of with all the radiosondes. These are radiosondes which are within 500 km of at least one of the GPS/MET soundings. Figure 9 shows the root mean square (r.m.s.) differences between the nearby radiosonde data and the GUESS field, as well as between the nearby radiosonde data and the analyses of ANGLE, NOGPS and BOTH. This comparison

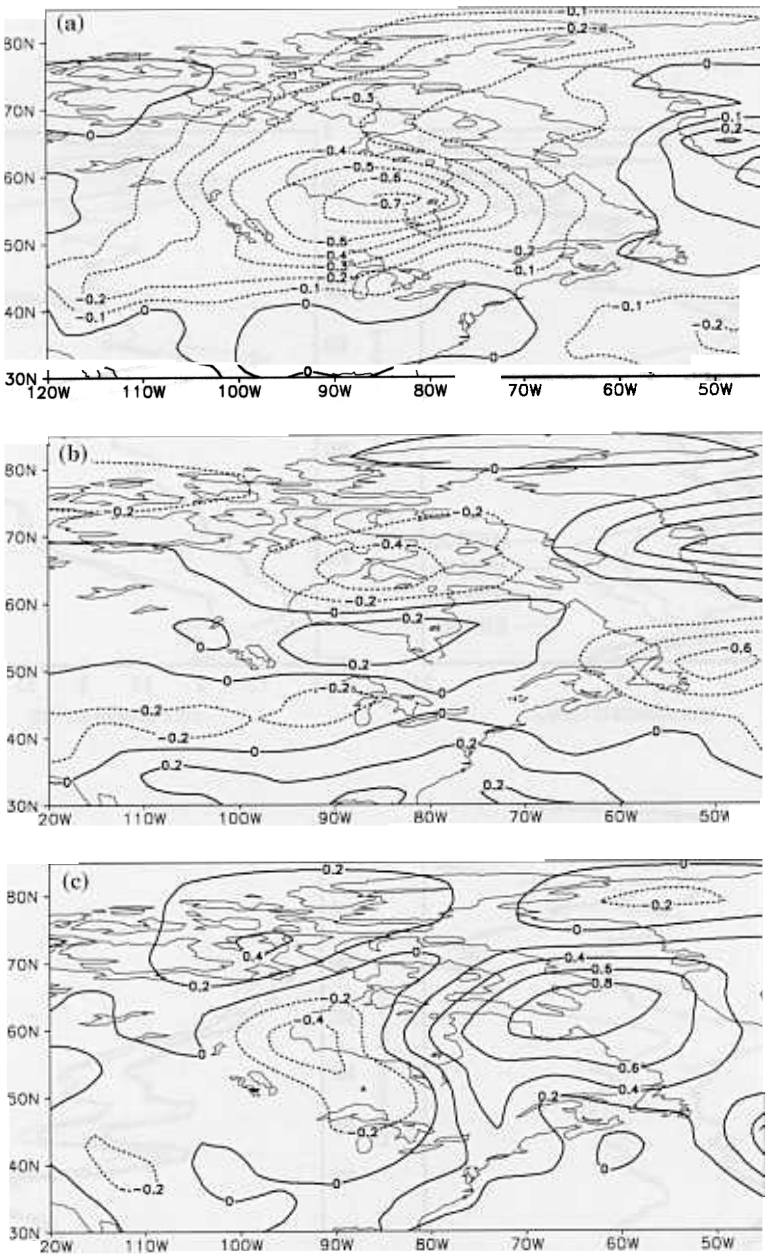

Figure 8. The ANGLE analysis increment of (a) temperature, (b) zonal wind, and (c) meridional wind at σ level 8 (approximately 850 hPa). Contour intervals are 0.1 degC for (a), and 0.2 m s^{-1} for (b) and (c). See text for further details.

includes a total of 28, 22, and 43 radiosonde stations for the temperature, specific humidity, and wind soundings, respectively. The fit of the temperature and wind (both the zonal wind and meridional wind components) of the ANGLE analysis to radiosondes (green lines) is improved over the GUESS field (black lines) except for the temperatures at levels between 530 and 670 hPa (Figs. 9(a), (b), and (c)). This represents a case in which the radiosonde data are withheld and used as independent analysis verification

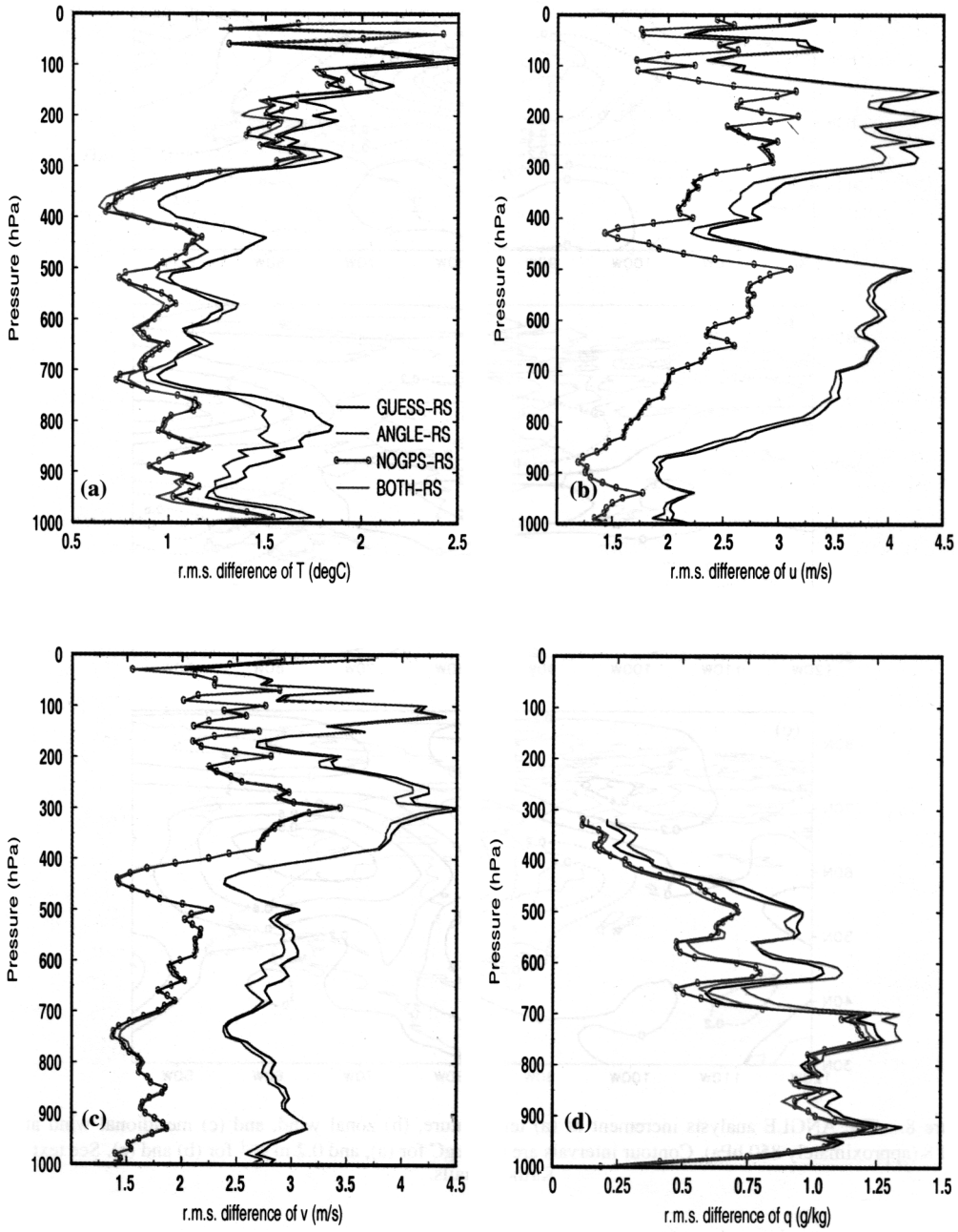

Figure 9. The root-mean-square (r.m.s.) difference between the nearby radiosonde data and the GUESS field (black line), ANGLE (green lines), NOGPS (blue lines), and BOTH (red lines) analyses. (a) temperature (T), (b) zonal wind (u), (c) meridional wind (v), (d) specific humidity (q). See text for further details.

data. The fit of the NOGPS (blue lines) and the BOTH (red lines) analyses to radiosonde measurements is much better than those of the GUESS field and the ANGLE analyses, as expected (NOGPS and BOTH include these radiosonde measurements). We notice that the fit of the ANGLE and BOTH specific-humidity analyses to radiosonde moisture measurements (Fig. 9(d)) shows a mixed result: a better fit of the ANGLE analysis than GUESS below 830 hPa and above 530 hPa, and a degraded result of the ANGLE analysis between 530 and 830 hPa. Similarly, a slightly improved fit of the BOTH analysis over the NOGPS analysis is observed below 830 hPa and above 530 hPa, and a slightly degraded fit of the BOTH analysis is observed between 530 and 830 hPa compared with the NOGPS analysis.

In summary, the use of a few (30 globally distributed) GPS/MET refraction angles in a 3D-Var analysis makes a small difference in the analysis of refractivity, temperature, water vapour and winds. However, even over data-rich regions (many radiosondes), and even when the verification data are the radiosondes themselves, the use of GPS/MET refraction angles makes a slight improvement overall to the analysed temperatures and winds. The moisture analysis shows mixed results, with improvements only below 830 hPa and above 530 hPa. These results are encouraging, given the large difference in the number and location of radiosonde and GPS observations. There are 500–600 radiosonde observations and only 30 GPS/MET observations. More than half (22) of the GPS observations are over data-sparse oceanic regions. One would not expect 30 GPS soundings to have much effect on the analyses interpolated to 500–600 radiosonde stations, especially since only 14 GPS soundings occurred within 500 km of a radiosonde observation. The use of the nearby radiosondes (Fig. 9) helps address the issue of the disparate number of observations, but the GPS observations are still typically 200–400 km away from the radiosonde points and there are differences in the times between the observations. The impact of GPS/MET data on global analysis thus depends very much on what is used for verification. In this study, the relative impact of radiosonde versus GPS/MET observations is heavily biased in favour of the radiosonde data.

(*d*) *Comparing the ANGLE1 analysis with nearby GPS/MET occultations*

The accuracy of the analysis using GPS/MET data cannot really be determined when the independent data for verification are not collocated in space and time with the GPS/MET data. It cannot be determined by using the same type of data when the data are sparse. In a data-rich area, however, some of the analysis errors can be assessed by comparing the analysis with observations that are withheld from the analysis. Fortunately, there are three occultations (GPS-1, GPS-2 and GPS-12) that are relatively close together, with a horizontal separation of 344 km between GPS-1 and GPS-2, 334 km between GPS-1 and GPS-12, and 593 km between GPS-2 and GPS-12. Figure 10 shows the horizontal distributions of the analysis increments to the specific-humidity fields at 850 hPa that resulted from the experiments ANGLE1, ANGLE2 and ANGLE12, which used the refraction angles of GPS-1, GPS-2 and GPS-12, respectively. The mean perigee-point positions of these three GPS occultations are indicated in Fig. 10(a). Both GPS-2 and GPS-12 are located within the analysis influence region of the GPS-1 occultation. The performance of the use of GPS/MET data in NCEP SSI analysis systems can thus be assessed by comparing the GUESS field and the ANGLE1 analysis with the observed GPS/MET refraction angles of GPS-2 and GPS-12. We find that the fit of the ANGLE1 analysis to GPS/MET refraction angles of both GPS-2 and GPS-12 is improved (comparing the first and the second lines of Table 3). Compared with the reduction of the differences between the simulated and the observed

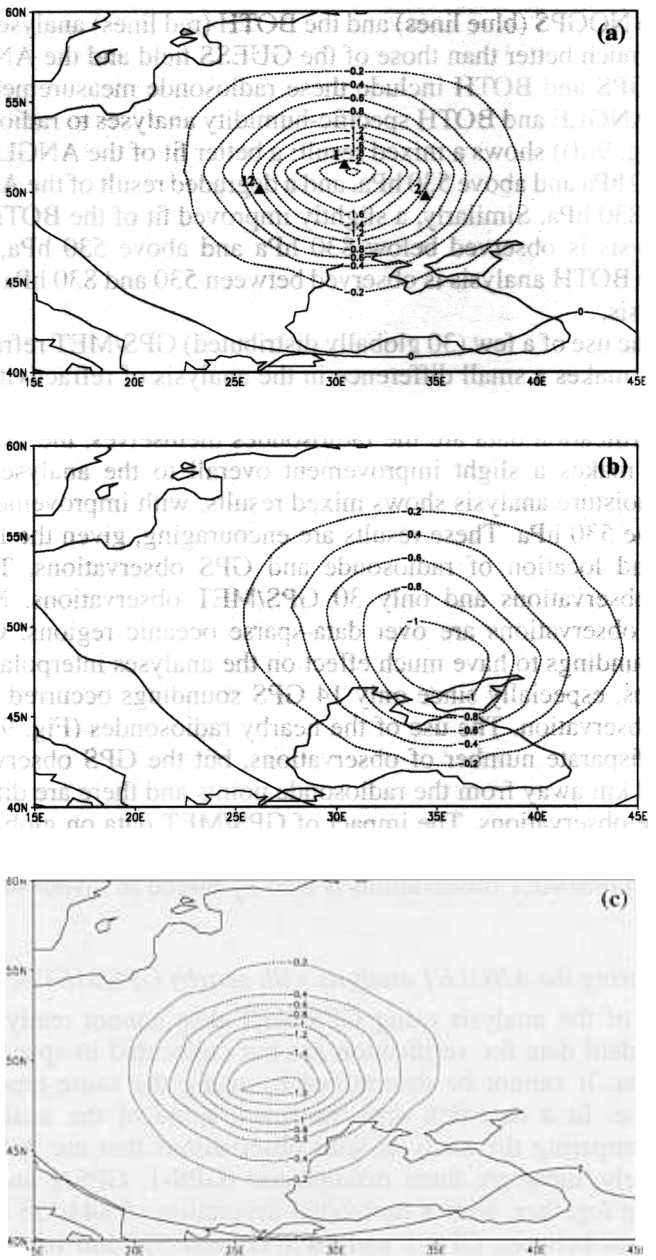

Figure 10. The horizontal distribution of the analysis increments of specific humidity at σ level 8 (approximately 850 hPa) for (a) ANGLE1, (b) ANGLE2, and (c) ANGLE12. Contour interval is 0.2 g kg^{-1}. See text for further details.

refraction angles of ANGLE2 (0.368×10^{-3} rad) and ANGLE12 (1.194×10^{-4} rad), such a fit of the ANGLE1 analysis to both GPS-2 and GPS-12 measurements is quite encouraging.

We can also compare the temperature and specific-humidity profiles at the GPS-2 and GPS-12 occultation locations among GUESS, ANGLE1, ANGLE2 and ANGLE12 analyses. Table 4 shows the r.m.s. differences in the temperature and specific-humidity

TABLE 3. THE ROOT-MEAN-SQUARE DIFFERENCES BETWEEN ANALYSES AND GPS-2 AND GPS-12 MEASUREMENTS, OVER ALL ALTITUDES

Analysis	GPS/MET observations	
	α of GPS-2 (10^{-3} rad)	α of GPS-12 (10^{-4} rad)
GUESS	1.134	4.436
ANGLE1	1.051	2.122
ANGLE2	0.368	3.864
ANGLE12	1.087	1.194

See text for further details.

TABLE 4. THE ROOT-MEAN-SQUARE DIFFERENCES BETWEEN THE ANGLE1 ANALYSIS AND THE ANALYSES FROM ANGLE2 AND ANGLE12, OVER ALL ALTITUDES

Verifying analyses	ANGLE2		ANGLE12	
	T (degC)	q (g kg^{-1})	T (degC)	q (g kg^{-1})
GUESS	0.5811	0.4382	0.4495	0.4386
ANGLE1	0.2587	0.3109	0.1934	0.0290

See text for further details.

analyses between the GUESS and the ANGLE2 (or ANGLE12) analysis, and those between the ANGLE1 analysis and the ANGLE2 (or ANGLE12) analysis at the GPS-2 and GPS-12 occultation locations. We find that the differences between ANGLE1 and ANGLE2 for both temperature and specific humidity are considerably smaller than the differences between GUESS and ANGLE2. Similar results are obtained when we compare GUESS and ANGLE1 with ANGLE12 at the GPS-12 occultation location. These results are encouraging, considering that the physical distance is still greater than 300 km between any two of the three selected occultations. This demonstrates the consistency between neighbouring retrievals of the 3D-Var assimilation of GPS/MET refraction-angle measurements, although it does not demonstrate the accuracy per se, due to the possible existence of potential sources of bias in these observations and/or their forward modelling.

Another indication from such an examination of the analyses of ANGLE1, ANGLE2 and ANGLE12 is that significant improvement to the analysis, over the entire globe, can be expected if the number of GPS occultations reaches an average horizontal resolution of less than 500 km over a 6 h time window. This requires about 16 LEO satellites assuming that each GPS receiver provides about 500 occultations per day (Rocken *et al.* 1997).

4. A MIXED USE OF GPS/MET REFRACTION ANGLES AND REFRACTIVITIES

The forward model used in this study for the GPS/MET refraction angles carried out the ray-tracing in a two-dimensional plane. It is much faster than an accurate 3D forward model. However, compared with other observations (e.g. TOVS radiance), the computational cost of the GPS forward model is still relatively high due to the required integration of the ray equation along each ray trajectory. For the present study, each occultation contains about 76 rays with the vertical resolution given in Table 1. The

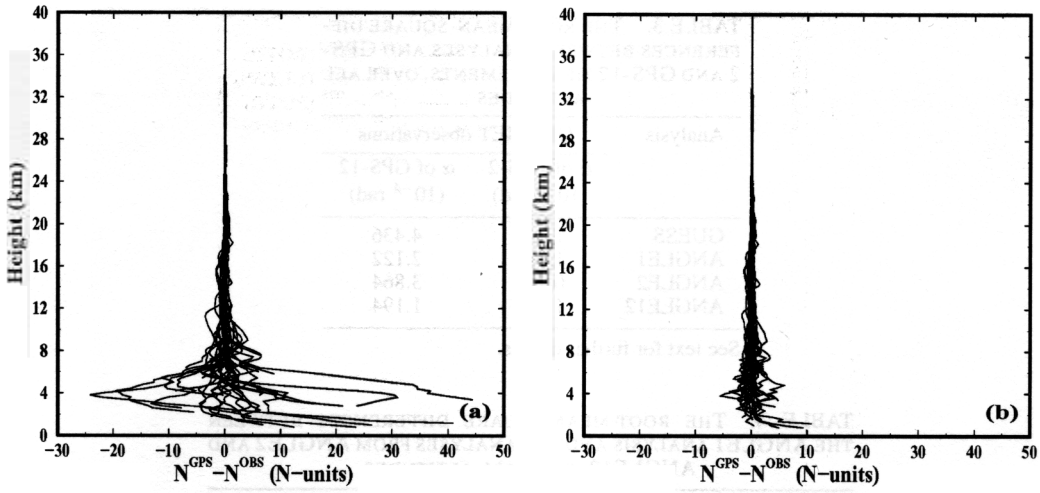

Figure 11 Spaghetti maps showing the 30 vertical profiles of $N^{GPS} - N^{OBS}$ for (a) GUESS and (b) BOTH. See text for further details.

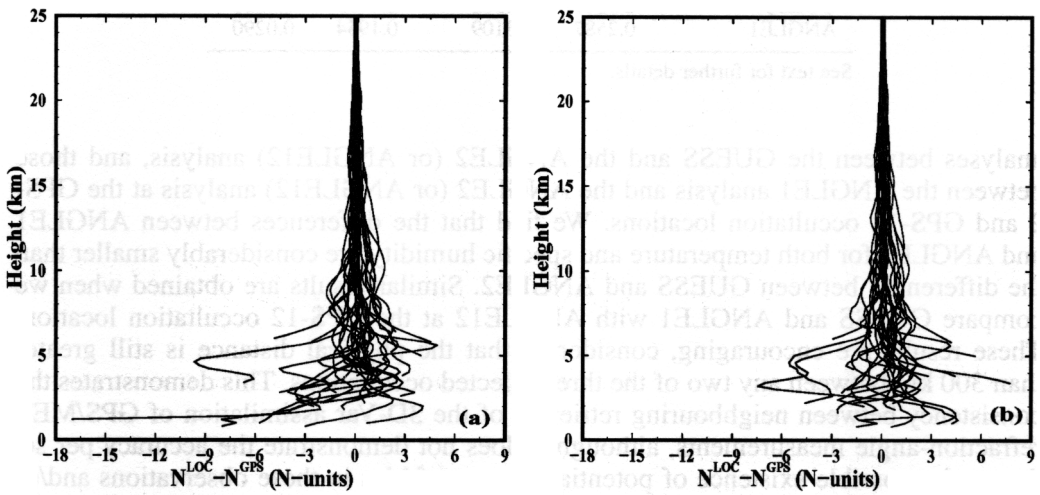

Figure 12. Same as Fig. 11 except for $N^{LOC} - N^{GPS}$. See text for further details.

forward model costs about 0.72 seconds for each occultation and 0.01 seconds for each ray (on CRAY3 at NCEP). We, therefore, adopt a strategy of using the refractivity instead of the refraction angle when the departure from spherical symmetry is small. First, a criterion for the use of refractivity instead of refraction angle at some points is selected. Then, the analysis produced by such a mixed use of refraction angle and refractivity is compared with the original analysis using refraction angles only.

We introduce the following notation:

N^{OBS}, the refractivities provided by POCC that were retrieved from the observed refraction angles using the Abel transform (Fjeldbo *et al.* 1971);

N^{GPS}, the refractivities derived using the Abel transform from refraction angles that have been simulated from the analysis fields using the forward ray-tracing operator; and

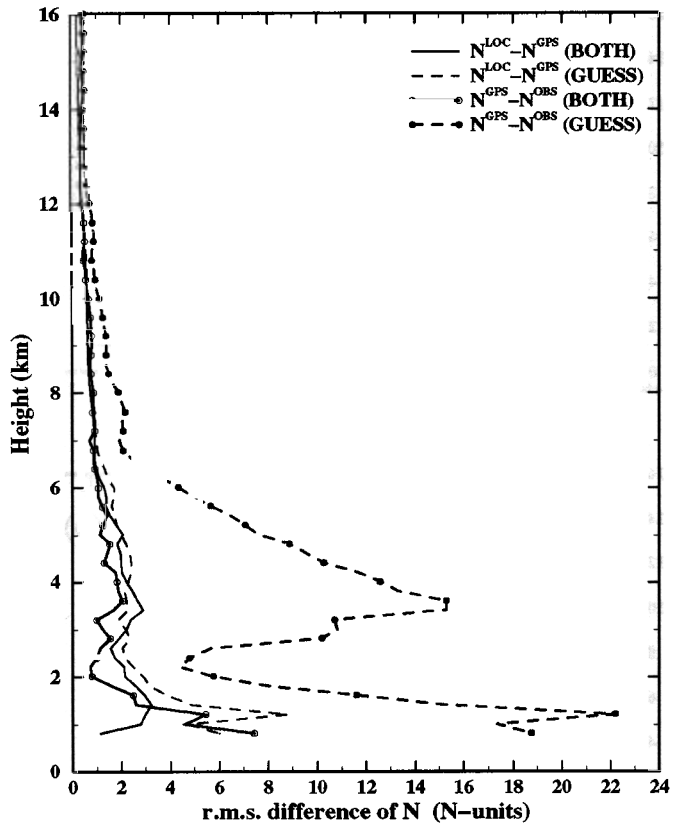

Figure 13. The vertical profiles of the root-mean-square (r.m.s.) difference between N^{GPS} and N^{OBS} and between N^{LOC} and N^{GPS} from GUESS and BOTH. See text for further details.

N^{LOC}, the refractivities calculated directly from the analysis fields (see Eq. (14) in Zou *et al.* 1999).

Figure 11 shows spaghetti maps of the 30 vertical profiles of $N^{GPS} - N^{OBS}$ from GUESS and BOTH. We find that the use of refraction angles significantly reduces the difference between N^{GPS} and N^{OBS}, especially below 7 km. This demonstrates the effectiveness of the use of refraction-angle data in making the analysis close to the observed GPS refractivity. The vertical profiles of the difference $N^{LOC} - N^{GPS}$, are shown in Fig. 12. Comparing Fig. 12(a) with Fig. 11(a), we find that the magnitude of the difference between N^{GPS} and N^{LOC} is, in general, smaller than the actual observational increment, $N^{GPS} - N^{OBS}$, calculated from the background field. The use of the GPS refraction angles significantly reduces the difference between N^{GPS} and N^{OBS} (Figs. 11(a) and (b)), but not $N^{LOC} - N^{GPS}$ (Figs. 12(a) and (b)). The vertical profiles of the mean absolute differences for $N^{GPS} - N^{OBS}$ and $N^{LOC} - N^{GPS}$ are shown in Fig. 13. We find that the differences between N^{LOC} and N^{GPS} are always smaller than the differences between N^{GPS} and N^{OBS} for the GUESS field, but not for the BOTH analysis in the low troposphere. Use of N^{OBS} without proper observational-error covariances (which is much more difficult to obtain than the use of refraction angles when spherical symmetry is not a good approximation) may not extract as much useful observational information as the use of refraction angles in the low troposphere.

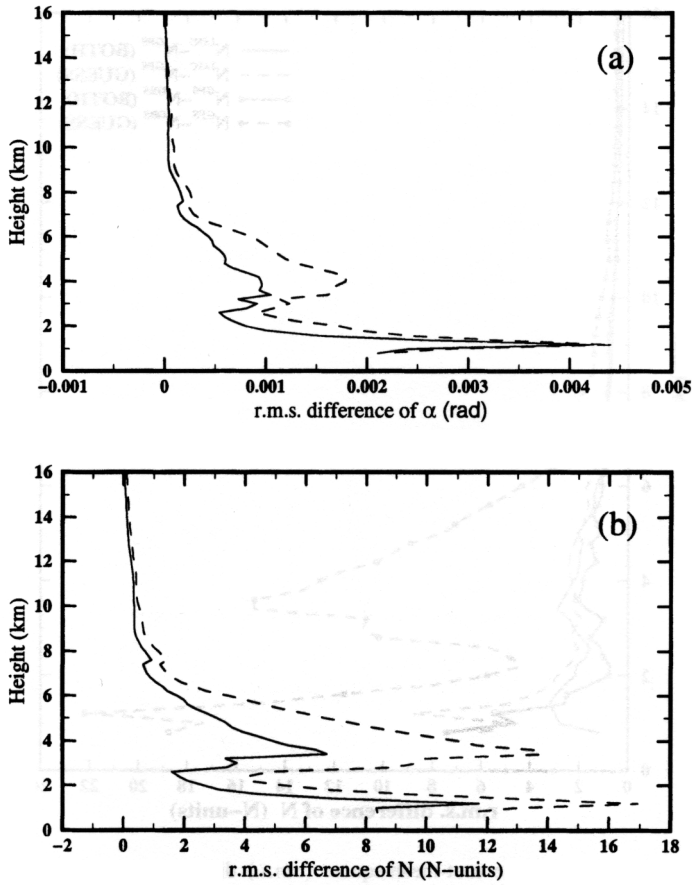

Figure 14. The root-mean-square (r.m.s.) difference of (a) refraction angles (α) and (b) refractivity (N) between REF and BOTH (solid line) and between GUESS and BOTH (dashed line). See text for further details.

Numerical results from an experiment identical to BOTH, except that refractivities, N^{OBS}, are used rather than refraction angles (REF), are presented in Fig. 14. The assumed observation errors in ln N^{OBS} (Fig. 15) are calculated in a similar manner to the use of refraction angles (see section 2). Similarly to Fig. 2(b), the vertical fluctuation in the structure of the observation error variance in the low troposphere may not be true and could have been caused by the very small sample used here.

Compared with BOTH, REF did quite well above 12.5 km but recovered only about half of the corrections that BOTH made to the GUESS field below 12.5 km. This implies that the use of GPS refractivity below 12.5 km is, in general, not sufficient to extract the maximum GPS observational information, probably due to the departure from the spherical symmetry of the atmospheric state. Since there are many more rays below 12.5 km than above (see Table 1 for the vertical sampling), the saving in the computational cost would be small if one had to use refraction angles below this height.

In order to maximize the impact of GPS data on analyses while minimizing the computational cost, we conduct two experiments for the mixed use of N^{OBS} and α^{OBS}. The selection between N^{OBS} and α^{OBS} at a perigee point is based on the differences between N^{GPS} and N^{LOC} calculated from the GUESS field. Two heights, $h_c^{(1)}$ and $h_c^{(2)}$,

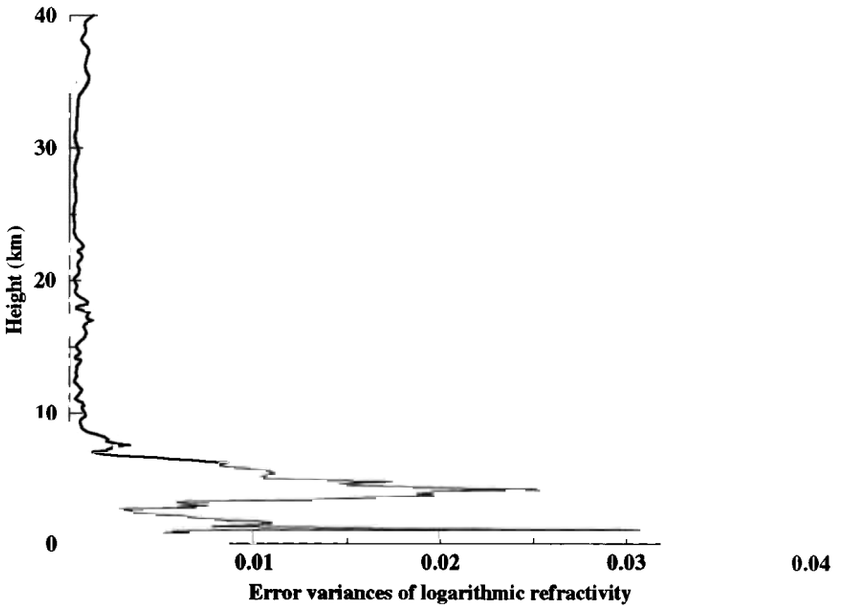

Figure 15 Variation of the estimated error variance of refractivity with height.

are calculated as follows:

$$|N^{\mathrm{LOC}} - N^{\mathrm{GPS}}|_{\text{guess field}} \begin{cases} < 0.25(\text{N-units}), & \text{if } h > h_c^{(1)} \\ \geqslant 0.25(\text{N-units}), & \text{if } h \leqslant h_c^{(1)} \end{cases} \tag{6}$$

and

$$h_c^{(2)} = \max(h_c^{(1)}, 7\ \text{km}) \tag{7}$$

where the threshold value of 0.25 N-units in Eq. (6) is the asymptotic value of the absolute r.m.s. differences between N^{LOC} and N^{GPS} as the height increases (see Fig. 13). For each occultation, refractivities and refraction angles are used above and below the height $h_c^{(1)}$ (MIXA) or $h_c^{(2)}$ (MIXB) (see Table 5). As in REF and BOTH, all the radiosondes are included in the analysis procedures of MIXA and MIXB. Results of these experiments are shown in Fig. 16. We observe that MIXA performs better than REF throughout the entire model level. Compared with BOTH, MIXA did very well above 7 km, but not as well below 7 km. The complicated moisture structures in the lower troposphere make $|N^{\mathrm{LOC}} - N^{\mathrm{GPS}}|_{\text{guess field}} < 0.25$ not an adequate indicator for the use of refractivity in the low troposphere. We, therefore, carried out an additional experiment (MIXB), which is similar to MIXA except that α^{OBS} is always used below 7 km. The MIXB analysis is more accurate than both REF and MIXA, and is very close to BOTH. Computational requirements for each of these experiments, summarized in Table 5, were based on calculations on CRAY3 at NCEP. The MIXB experiment uses 31% less central-processing-unit time compared with BOTH, performs better than both REF and MIXA, and results in a similarly accurate analysis to BOTH when compared with the GPS/MET observed refraction angles (α^{OBS}) and the GPS-derived refractivity (N^{OBS}).

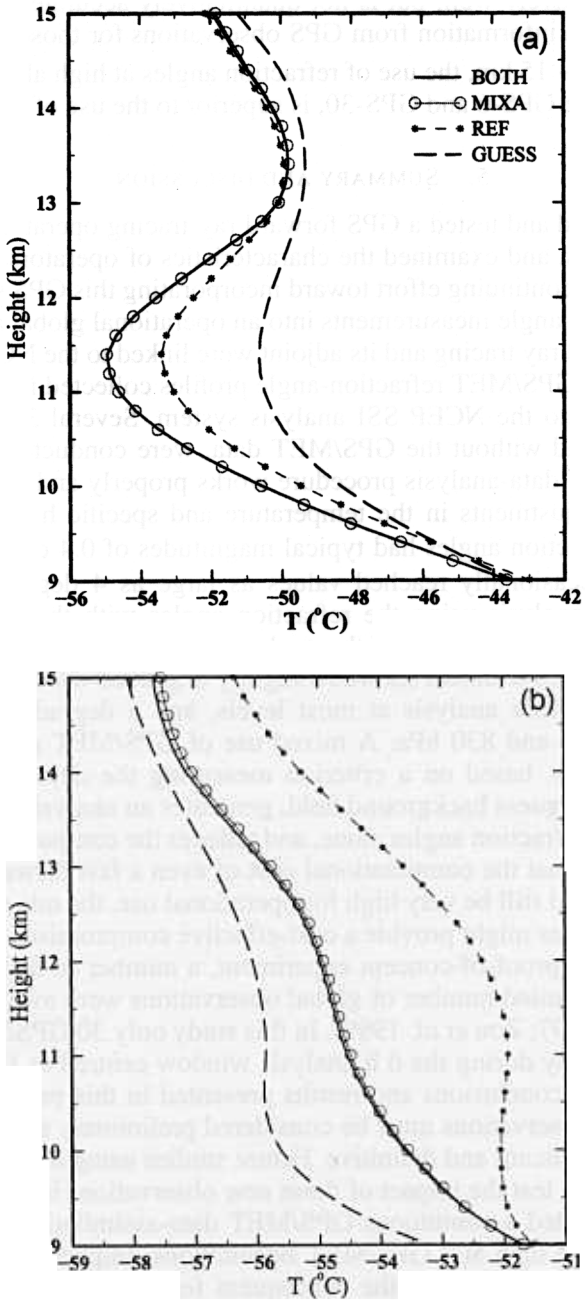

Figure 17. The temperature profiles at the locations of (a) GPS-6 and (b) GPS-30 from the analyses of BOTH, MIXA, REF, and GUESS. See text for further details.

are closer to those of BOTH than REF. In particular, the temperature inversion at the GPS-6 occultation location, seen in BOTH, is recovered exactly in MIXA. The use of GPS refractivity observations at these levels (from 9 km to 15 km) enables recovery of this structure qualitatively well, but is not quantitatively accurate enough. In order to extract the maximum information from GPS observations for those types of soundings for which $h_c^{(1)} > 12 - 15$ km, the use of refraction angles at high altitudes, as is done in MIXA and MIXB for GPS-6 and GPS-30, is superior to the use of refractivities.

5. Summary and discussion

Having developed and tested a GPS forward ray-tracing operator, its tangent linear and adjoint operators, and examined the characteristics of operators (Zou *et al.* 1999), this paper presents a continuing effort toward incorporating this GPS software and these GPS/MET refraction-angle measurements into an operational global analysis system.

The GPS forward ray tracing and its adjoint were linked to the NCEP SSI system. A total of 30 observed GPS/MET refraction-angle profiles collected in a 6 h time window were incorporated into the NCEP SSI analysis system. Several 3D-Var data-analysis experiments, with and without the GPS/MET data, were conducted. The experiments showed that the GPS data-analysis procedure works properly and fits the observations reasonably well. Adjustments in the temperature and specific humidity that resulted from the use of refraction angles had typical magnitudes of 0.4 degC and 0.6 g kg^{-1}, respectively, but occasionally reached values as large as 4 degC and 4 g kg^{-1}. A comparison of the analysis using the refraction angles with the nearby radiosondes showed mixed results. Verification of the analysis using the refraction angles with the radiosonde observations withheld showed a slightly improved wind analysis at all levels, an improved temperature analysis at most levels, and a degraded specific-humidity analysis between 530 and 830 hPa. A mixed use of GPS/MET refraction angles and GPS/MET refractivity, based on a criterion measuring the departure from spherical symmetry of the first-guess background field, generates an analysis of similar accuracy to the one using the refraction angles alone, and reduces the computational cost by about 30%. Given the fact that the computational cost of even a fast forward model for GPS refraction angles could still be very high for operational use, the mixed use of refraction angles and refractivities might provide a cost-effective compromise.

In the GPS/MET proof-of-concept experiment, a number of factors contributed to the fact that only a limited number of global observations were available on any given day (Rocken *et al.* 1997; Zou *et al.* 1999). In this study only 30 GPS/MET observations were available globally during the 6 h analysis window centred at 12 UTC 11 October 1995. Therefore, the conclusions and results presented in this paper pertaining to the impact of these 30 observations must be considered preliminary and illustrative, rather than statistically significant and definitive. Future studies using much larger GPS/MET datasets are needed to test the impact of these new observations in a definitive way. We have recently conducted a continuous GPS/MET data-assimilation cycle for a period of 11 days with more than 800 GPS/MET occultations. Impacts of these data on the large-scale analysis, and possibly the subsequent forecasts, are being analysed. An observing-system simulation experiment may also help to assess the potential impact of GPS occultation measurements on global analyses and forecasts.

Several international projects include plans to launch many more LEO satellites equipped with GPS receivers. It is anticipated that larger impacts on global analyses will occur when more GPS measurements are made available through these efforts, and problems associated with the use of GPS data are further investigated.

ACKNOWLEDGEMENTS

This research is supported by the Integrated Program Office of the National Oceanic and Atmospheric Administration National Polar-orbiting Operational Environmental Satellite System (NPOESS) under Project Order No. Q000C1737600086, the National Science Foundation under project No. ATM-9812729, and Chinese Excellent Funding 49825109. The authors would like to thank S. Lord, J. Derber, J. Sela, R. Treaton, and W.-S. Wu at NCEP for the generous help they provided during the course of this work.

REFERENCES

Andersson, E., Haseler, J., Undén, P., Courtier, P., Kelly, G., Vasiljević, D., Branković, C., Gaffard, A., Hollingsworth, A., Jakob, C., Janssen, P., Klinker, E., Lanzinger, A., Miller, M., Rabier, F., Simmons, A., Strauss, B., Thépaut, J.-N. and Viterbo, P. 1998 The ECMWF implementation of three-dimensional variational assimilation (3D-Var). III: Experiment results. *Q. J. R. Meteorol. Soc.*, **124,** 1831–1860

Cacuci, D. G. 1981 Sensitivity theory for nonlinear systems. I: Nonlinear functional analysis approach. *J. Math. Phys.*, **22,** 2794–2802

Courtier, P., Andersson, E., Heckley, W., Pailleux, J., Vasiljević, D., Hamrud, M., Hollingsworth, A., Rabier, F. and Fisher, M. 1998 The ECMWF implementation of three-dimensional variational assimilation (3D-Var). I: Formulation. *Q. J. R. Meteorol. Soc.*, **124,** 1783–1808

Courtier, P., Thépaut, J.-N. and Hollingsworth, A. 1994 A strategy for operational implementation of 4D-VAR, using an incremental approach. *Q. J. R. Meteorol. Soc.*, **120,** 1367–1387

Eyre, J. R. 1994 'Assimilation of radio occultation measurements into a numerical weather prediction system'. ECMWF Technical Memo. 199. European Centre for Medium-Range Weather Forecasts, Reading, UK

Fjeldbo, G., Kliore, G. A. and Eshleman, V. R. 1971 The neutral atmosphere of Venus as studied with the Mariner V radio occultation experiments. *Astron. J.*, **76,** 123–140

Hocke, K. 1997 Inversion of GPS meteorology data. *Ann. Geophys.*, **15,** 443–450

Kuo, Y.-H., Zou, X. and Huang, W. 1997 The impact of GPS data on the prediction of an extratropical cyclone: An observing system simulation experiment. *J. Dyn. Atmos. Ocean.*, **27,** 439–470

Kursinski, E. R., Hajj, G. A., Bertiger, W. I., Leroy, S. S., Meehan, T. K., Romans, L. J., Schofield, J. T., McCleese, D. J., Melbourne, W. G., Thornton, C. L., Yunck, Y. P., Eyre, J. R. and Nagatani, R. N. 1996 Initial results of radio occultation observations of Earth's atmosphere using the global positioning system. *Science*, **271,** 1107–1110

Kursinski, E. R., Hajj, G. A., Schofield, J. T., Linfield, R. P. and Hardy, K. R. 1997 Observing Earth's atmosphere with radio occultation measurements using the Global Positioning System. *J. Geophys. Res.*, **102,** 23429–23465

Le Dimet, F. X. and Talagrand, O. 1986 Variational algorithms for analysis and assimilation of meteorological observations: Theoretical aspects. *Tellus*, **38A,** 97–110

Navon, I. M., Zou, X., Derber, J. and Sela, J. 1992 Variational data assimilation with an adiabatic version of the NMC spectral model. *Mon. Weather Rev.*, **120,** 1433–1446

Parrish, D. F. and Derber, J. C. 1992 The National Meteorological Center's spectral statistical-interpolation analysis system. *Mon. Weather Rev.*, **120,** 1747–1763

Rabier, F., McNally, A., Andersson, E., Courtier, P. Undén, P., Eyre, J., Hollingsworth, A. and Bouttier, F. 1998a The ECMWF implementation of three-dimensional variational assimilation (3D-Var). II: Structure functions. *Q. J. R. Meteorol. Soc.*, **124,** 1809–1830

Rabier, F., Thépaut, J.-N. and Courtier, P. 1998b Extended assimilation and forecast experiments with a four-dimensional variational assimilation system. *Q. J. R. Meteorol. Soc.*, **124,** 1861–1887

Rocken, C., Anthes, R., Exner, M., Hunt, D., Sokolovskiy, S., Ware, R., Gorbunov, M., Schreiner, W., Feng, D., Herman, B., Kuo, Y.-H. and Zou, X. 1997 Analysis and validation of GPS/MET data in the neutral atmosphere. *J. Geophys. Res.*, **102,** 29849–29866

Tsuda, T., Nishida, M., Rocken, C. and Ware, R. H. 2000 A global morphology of gravity wave activity in the stratosphere revealed by the GPS occultation data (GPS/MET). *J. Geophy. Res.*, **105,** 7257–7273

Ware, R., Exner, M., Feng, D., Gorbunov, M., Hardy, K., Herman, B., Kuo, Y.-H., Meehan, T., Melbourne, W., Rocken, C., Schreiner, W., Sokolovskiy, S., Solheim, F., Zou, X., Anthes, R., Businger, S. and Trenberth, K. 1996 GPS sounding of the atmosphere from low earth orbit: Preliminary results. *Bull. Am. Meteorol. Soc.*, **77,** 19–40

Zou, X., Barcilon, A., Navon, I. M., Whitaker, J. and Cacuci, D. G. 1993 An adjoint sensitivity study of blocking in a two-layer isentropic model. *Mon. Weather Rev.*, **121,** 2833–2857

Zou, X., Kuo, Y. H. and Guo, Y.-R. 1995 Assimilation of atmospheric radio refractivity using a nonhydrostatic adjoint model. *Mon. Weather Rev.*, **123,** 2229–2249

Zou, X., Vandenberghe, F., Wang, B., Gorbunov, M. E., Kuo, Y.-H., Sokolovskiy, S., Chang, J. C., Sela, J. G. and Anthes, R. A. 1999 A raytracing operator and its adjoint for the use of GPS/MET refraction angle measurements. *J. Geophys. Res.*, **104,** 22301–22318

Zupanski, M. and Zupanski, D. 1995 'Recent development of NMC's regional four-dimensional variational data assimilation system.' Pp. 367–372 in Proceedings of the Second International Symposium on Assimilation of Observations in Meteorology and Oceanography, Tokyo, Japan. WMO